Oxidation of Metals, Vol. 5, No. 2, 1972

A Review of the Diffusion Path Concept and Its Application to the High-Temperature Oxidation of Binary Alloys

A. D. Dalvi*† and D. E. Coates*‡

Received August 17, 1970—Revised August 24, 1972

Ternary diffusion theory, particularly the concept of diffusion paths on a ternary phase diagram, is reviewed in terms of its application to the problem of binary alloy oxidation. To illustrate this applicability, the oxidation behavior of Fe–Ni, Fe–Cr, and Ni–Cr alloys at 1000°C is examined in detail.

INTRODUCTION

A theoretical description of the high temperature oxidation behavior of binary alloys must consider the diffusional processes taking place in both the oxide scale and the alloy. Since three species are involved (i.e., the alloying elements A and B, and oxygen O), a completely general description must also involve the elements of ternary diffusion theory. At high temperatures, one can usually assume that a condition of local thermodynamic equilibrium prevails at the gas–scale and scale–alloy interfaces. The requirement that the various diffusing species be conserved at the interfaces and the local equilibrium conditions leads to a coupling or interdependence of the diffusion fields in the oxide and alloy phases. This interplay between diffusion in the two phases involves thermodynamic as well as kinetic considerations. It follows that a knowledge of the thermodynamics of the ternary system A-B-O, preferably in the form of a ternary phase diagram, is a necessity.

*Department of Metallurgy and Materials Science, McMaster University, Hamilton, Ontario, Canada.

†Present address: J. Roy Gordon Research Laboratory, The International Nickel Company of Canada Ltd., Sheridan Park, Mississauga, Ontario, Canada.

‡Present address: Department of Metallurgy, The University of British Columbia, Vancouver, B.C., Canada.

It is the opinion of the present authors that the most effective means of representing the relationship between the kinetic and thermodynamic aspects of binary alloy oxidation and the corresponding oxide scale and subscale structures is by means of a diffusion path on the appropriate A-B-O ternary isotherm. The terms diffusion path, diffusion composition path, composition path, and locus of compositions have been used at various times and have essentially equivalent meaning. In the past, this approach to the binary alloy oxidation problem has not enjoyed very widespread use. The three principal reasons for this are: (a) until recently there have not been any reliable ternary constitutional diagrams of the A-B-O- type, (b) only in the past ten years have the principles of multicomponent diffusion theory been clearly elucidated and (c) it has become possible, only recently, to measure concentration profiles in the alloy and oxide phases (with the aid of an electron microprobe analyzer). Now that data on phase equilibria in ternary A-B-O systems are rapidly accumulating and the theory of ternary diffusion is well developed, the ternary diffusion path approach can be seriously considered as a means of examining binary alloy oxidation behavior.

In the present article, ternary diffusion theory and, in particular, the concept of a diffusion path on a ternary phase diagram are reviewed. These concepts are then applied in an examination of the oxidation behavior of Fe–Ni, Fe–Cr, and Ni–Cr alloys at 1000°C.

HISTORICAL BACKGROUND

In 1940, Rhines[1] made use of A-B-O type phase diagrams in an attempt to predict the sequence of oxide layer formation during the oxidation of copper alloys. He used the expedient of drawing, upon the appropriate A-B-O ternary isotherm, a straight line connecting the oxygen corner to the bulk AB alloy composition and then noting the order and identity of the one-phase and two-phase regions crossed. Rhines was quite aware that the assumption of a linear composition path was an oversimplification. Nevertheless, using this approach he was able to indicate how scale structure depends on bulk alloy composition.

Thomas[2] studied the high temperature oxidation of Cu–Pd and Cu–Pt alloys. On the basis of observed scale and subscale structures corresponding to various bulk alloy compositions, he proposed diffusion paths* on the appropriate schematic ternary isotherm. On this basis, Thomas was able to interpret the five modes of oxidation scale structure which he observed for Cu–Pd alloys.

*He used the term locus of compositions.

Using metallographic and x-ray diffraction methods, Clark and Rhines[3] studied the identity, order, and structure of ternary diffusion layers for diffusion couples composed of Al and a series of six Mg–Zn alloys. On the basis of these results, they postulated fourteen general rules governing the course of diffusion paths corresponding to multilayered ternary diffusion structures. A few of these rules have subsequently been shown to be incorrect.

Kirkaldy and Brown[4] established general principles for the description of diffusion structures in ternary systems. These authors developed a set of seventeen general theorems or rules pertaining to the construction of diffusion paths on a ternary isotherm. They also introduced the concept of "virtual path" as an aid to path prediction in multiphase systems. Reference 4 offers a good summary of fundamental principles which can be readily applied to oxide scale and subscale formation during binary alloy oxidation.

TERNARY DIFFUSION EQUATIONS

At this juncture, it is worthwhile outlining certain elementary concepts pertaining to ternary diffusion theory. A more detailed discussion of ternary diffusion and its relation to oxidation and sulfidation is to be found in recent review articles by Kirkaldy.[5,6]

For ternary systems, Onsager[7] has suggested the following generalization of Fick's first law

$$J_1 = -D_{11}\nabla C_1 - D_{12}\nabla C_2 \tag{1}$$

$$J_2 = -D_{21}\nabla C_1 - D_{22}\nabla C_2 \tag{2}$$

where C_1 and C_2 are molar concentrations and D_{11}, D_{22}, D_{12} and D_{21} are diffusion coefficients. Recognizing that the fundamental driving forces for isothermal diffusion are chemical potential gradients, not concentration gradients, one can relate the above D's to the appropriate chemical potentials and to a set of phenomenological coefficients which evolve out of the thermodynamics of irreversible processes.[7–11] The volume-fixed reference frame is defined by the condition

$$\overline{V}_1 J_1 + \overline{V}_2 J_2 + \overline{V}_3 J_3 = 0 \tag{3}$$

where $\overline{V}_1$, $\overline{V}_2$, and $\overline{V}_3$ are partial molar volumes. Clearly, the flux of component 3 can be regarded as dependent (i.e., one regards 3 as the solvent).

D_{11} and D_{22} are measures of the influence of the concentration gradient of a given component on its own flux, whereas D_{12} and D_{21} reflect interference or cross effects. For example, D_{12} is a measure of the ability of the

distribution of component 2 to influence the distribution of component 1. D_{12} and D_{21} usually have the same algebraic sign. To say that in a ternary system there is significant diffusional interaction is to imply that either or both of $D_{12}\nabla C_2$ and $D_{21}\nabla C_1$ are significant in magnitude relative to $D_{11}\nabla C_1$ and $D_{22}\nabla C_2$, respectively, in Eqs. (1) and (2).

In view of the relevance to binary alloy oxidation, consider transport in an AB substitutional alloy which contains dissolved oxygen. Let component 3 be regarded as the solvent alloying element, component 2 as the solute, and component 1 as oxygen. Since oxygen predominantly moves by an interstitial mechanism, $D_{11} \gg D_{22}$ and the distribution of component 1 is very flat relative to that of component 2, i.e.,

$$\nabla C_1 \ll \nabla C_2 \tag{4}$$

It follows that, from condition (4) and the fact that in general $|D_{21}| < D_{22}$, $|D_{22}\nabla C_2| \gg |D_{21}\nabla C_1|$ in Eq. (2). That is to say, the distribution of oxygen has negligible influence on the distribution of the alloy solute. On the other hand, although $|D_{12}| < D_{11}$, it is quite possible that if condition (4) is extreme, $D_{12}\nabla C_2$ could dominate $D_{11}\nabla C_1$ in Eq. (1). Thus the distribution of the alloy solute could have a very significant influence on the oxygen distribution. This effect could be very important in dealing with the phenomenon of internal oxidation. Kirkaldy and Purdy[12] have demonstrated that if component 1 is a relatively dilute interstitial and component 2 is a dilute substitutional element, then

$$\frac{D_{12}}{D_{11}} \simeq \left.\frac{\partial \ln \gamma_1}{\partial X_2}\right|_{X_1, X_2 = 0} X_1 = \varepsilon_{12} X_1 \tag{5}$$

where X_1 and X_2 are mole fractions, γ_1 is the activity coefficient of component 1, and ε_{12} is the Wagner interaction coefficient. Equations (1) and (5) demonstrate that diffusional interaction in alloys involving dilute amounts of a substitutional solute and oxygen is essentially a manifestation of thermodynamic interaction between these species.

DIFFUSION PATHS ON TERNARY A-B-O ISOTHERMS

Progressively more refined theoretical treatments of the binary alloy oxidation problem have been presented over the years, notably by Rhines *et al.*,[13] Thomas,[2] and Wagner.[14–18] These analyses attempt to predict the concentration distributions in the scale, subscale, and alloy, as well as the scale and subscale thickening rates. Wagner's most recent study is of particular interest since it considers the generalized situation in which the metals A and B react with oxygen to form a scale consisting of a solid

solution of the corresponding oxides. For further discussion of this analysis the reader is referred to Refs. 19 and 20.

For the purposes of the present article it is assumed that the various concentration distributions (corresponding to binary alloy oxidation) have been determined theoretically using treatments similar to those just cited, or have been determined experimentally, for example, by electron microprobe analysis. Our interest is in how these distributions can be related to the ternary phase diagram.

Consider as an initial example, the simple case in which a single oxide $A_{n-x}B_xO$ forms on the binary alloy AB. There are assumed to be no restrictions on the solubility of B in the oxide or that of O in the alloy. From the Gibbs' phase rule it follows that the concentration of one of the components is dependent, for the isothermal and isobaric conditions that are assumed. In Fig. 1 concentration distributions in moles per unit volume of the arbitrarily chosen independent components A and O are shown schematically for time t.

In the most general case, the distributions C_A and C_O are functions of distance and time. If it can be shown that C_A and C_O are parametric solutions to the diffusion equations (that is, for all values of distance (x) and time (t), $C_A = C_A(\lambda)$ and $C_O = C_O(\lambda)$ where λ is a function of x and t) then elimination of λ between these expressions will yield a distance and time-independent relation

$$C_A = C_A(C_O) \tag{6}$$

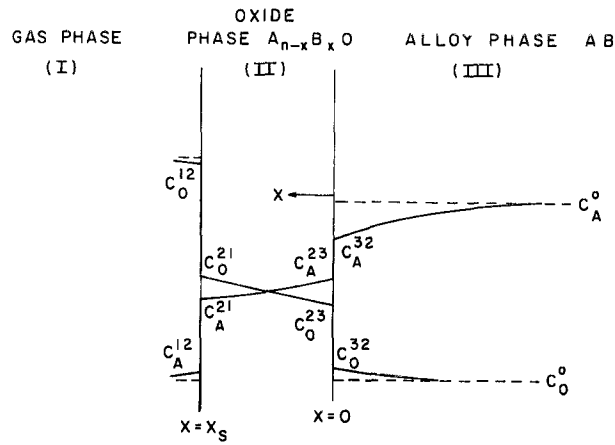

Fig. 1. Schematic representation of the independent concentration distributions in the gas, oxide, and alloy phases. The nomenclature for the interfacial concentrations is arranged so that C_i^{jk} is the concentration of component i (A or O) in phase j at the interface adjacent to phase k.

The plot of this relation on the corresponding ternary phase diagram, the path O-Q in Fig. 2, will therefore be stationary in time. For transformations which are diffusion controlled and involve infinite or semiinfinite boundary conditions, the parametric substitution

$$\lambda = xt^{-1/2} \tag{7}$$

is valid and this leads to the familiar parabolic oxidation kinetics. The invariant path O-Q is the diffusion path and it is unique for the given terminal compositions and given set of experimental conditions, e.g., temperature, pressure, etc.[4]

When the oxidation process is diffusion controlled and therefore the concentration distributions are parametric in distance and time, the interfacial concentrations (C_A^{12}, C_O^{12}), (C_A^{21}, C_O^{21}), (C_A^{23}, C_O^{23}), (C_A^{32}, C_O^{32}) are independent of time. However, these concentrations are not known *ab initio*; rather they are obtained as part of the solution to the diffusion equations. This is quite unlike isothermal oxidation of a pure metal in which case the binary phase diagram uniquely specifies the interface concentrations if local equilibrium is assumed to prevail at the interfaces.

If the diffusion path is obtained from calculations based on diffusion models which involve only planar interfaces and an assumed sequence of single-phase regions, then it may have to be regarded as being a "virtual" diffusion path.[4] For example, assume the calculated path dips from a single-phase field into a two-phase field, thereby cutting tie lines, and returns to the single-phase region. This path is a "virtual" one since the situation is unstable, in view of the isolated zone of supersaturated material. The actual

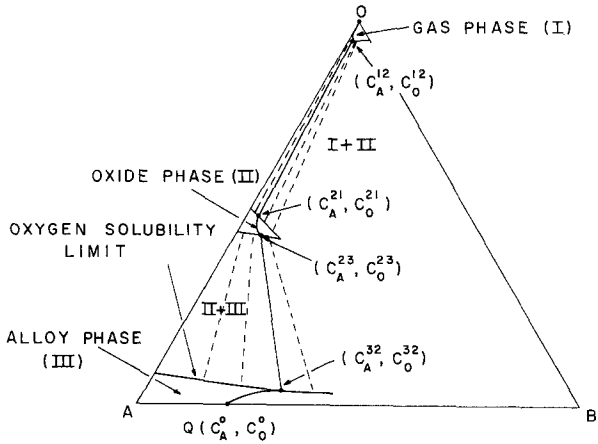

Fig. 2. Schematic representation of an isothermal phase diagram on which is superimposed the "virtual" diffusion path O-Q.

diffusion path may involve nonplanar interfaces or internal precipitates or both. These develop in an effort to eliminate the supersaturation. On the other hand, if the calculated diffusion path does not enter a two-phase field, other than to cross coincident with a tie line, then this path will coincide with the actual (experimentally observed) diffusion path if no kinetic instability occurs.

Because there are so little equilibrium and diffusion data available for the oxide phase regions of ternary A-B-O type diagrams, it is not usually realistic to attempt to calculate virtual diffusion paths through these regions. Therefore actual diffusion paths, corresponding to the observed scale microstructures, are used for that part of diffusion paths. However, meaningful diffusion paths for the alloy phase can be calculated, and hence, these are employed for the part of diffusion paths within the alloy phase. As better data and better theoretical models become available, it may be possible to calculate diffusion paths corresponding to two-phase regions.

In their examination of ternary diffusion layer formation, Clark and Rhines[3] give a very useful summary of the relationship between observed diffusion structure and the corresponding phase diagram. Table I is based on that summary.

It was mentioned earlier that Kirkaldy and Brown[4] give a list of 17 theorems pertaining to the construction of ternary diffusion paths. In the

Table I. Diffusion Structures and Course of Diffusion Path on Corresponding Phase Diagram

Diffusion structure	Diffusion path
Single-phase layer	Traversing a single-phase field.
Two-phase layer	Traversing a two-phase field by cutting tie lines. Ratio of phases indicated by positions at which tie lines cut and equilibrium concentrations by ends of tie lines.
Interface: single-phase–single-phase	Traversing a two-phase field parallel with a tie line. Interface concentrations given by ends of the tie line.
Interface: single-phase–two-phase (two phases altogether)	Traversing the boundary between a single-phase and two-phase field, cutting tie lines in latter.
Interface: single-phase–two-phase (three phases altogether)	Traversing a three-phase field from corner to side, the position on the side being indicated by the two-phase ratio.
Interface: two-phase–two-phase (three phases altogether)	Traversing a three-phase field from side to side, the position on each side being indicated by the corresponding two-phase ratio.

following list, the more relevant of these rules are given in terms of how they apply to binary alloy oxidation. It is assumed that there is no evaporation of the alloying elements A and B and, for simplicity, that the atmospheric oxygen potential is unity.

a. The shift in the alloy composition from the bulk alloy to the alloy–oxide interface is away from the component which is preferentially oxidized.
b. The diffusion path must, at least once, cross the straight line joining the oxygen corner of the phase diagram to the bulk alloy composition.
c. At a given temperature, the diffusion path is defined uniquely only by the bulk alloy composition.
d. In order to maintain monotonic activity gradients, a diffusion path in a two-phase region cannot reverse its order of crossing tie lines.
e. To the extent that the effect of lateral diffusion and nonplanar interfaces can be ignored or averaged out, the diffusion paths involving two-phase regions are time invariant.

INTERNAL OXIDATION

Let us assume that the virtual diffusion path corresponding to a binary alloy oxidation situation has been calculated. Two possibilities are shown in Fig. 3. Because the calculated diffusion path for the alloy cuts tie lines in the two-phase field in case (b), it is clear that a region of "constitutional" supersaturation would be developed in the alloy adjacent to a planar alloy–oxide interface. Relief of the supersaturation can occur through morphological breakdown of the planar alloy–oxide interface* and/or

†That is, by a transition from a planar to nonplanar interface shape, in analogy with the planar to cellular solid–liquid interface transition associated with constitutional supercooling.[21,22]

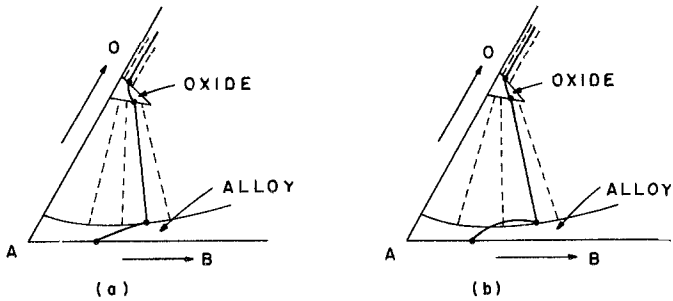

Fig. 3. (a) "Virtual" diffusion path which does not involve a supersaturation region in the alloy. (b) "Virtual" diffusion path which does involve a supersaturation region in the alloy.

through internal precipitation of oxide within the alloy phase adjacent to the interface (i.e., through internal oxidation). In either case, the calculated concentration distributions (and corresponding virtual diffusion path) are no longer valid. Because no zone of supersaturation is developed, Fig. 3(a) represents a stable configuration for which the virtual and actual diffusion paths are coincident.

It should be noted that in systems of the form A-B-O, there is a significant tendency to form a zone of supersaturation in the alloy adjacent to the scale–alloy interface. The rather high diffusivity of O, relative to B, results in the former species having a much shallower interface concentration gradient than the latter component. This in turn means the slope of the virtual diffusion path in the alloy, at the scale–alloy interface, approaches zero. This is precisely the situation which is required in order to cut into the two-phase field and produce supersaturation (see Fig. 3).

A virtual diffusion path which involves a zone of supersaturation, in effect, predicts the existence of configurations involving two-phase (oxide–alloy) regions. The actual diffusion path is calculated by taking such predictions into account and reformulating the problem in such a way as to involve the appropriate two-phase regions. Thus if there is a zone of internal precipitation within the alloy, the essential (and difficult) problem is to determine the concentration distributions in the precipitate and matrix for this zone. Numerous quantitative treatments have been attempted, some of the more important of which are due to Rhines *et al.*,[13] Darken,[23] Thomas,[2] Wagner,[17,24] Kahlweit *et al.*,[25–27] and Kirkaldy.[6,28] Rapp[29] has recently reviewed the subject of internal oxidation. Once the matrix concentration distributions for the precipitate zone of the alloy are known, the overall problem is a slight complication of that represented in Fig. 1. At the interface between the precipitate zone and precipitate-free alloy, $x = x_P$, there are three unknowns, C_O^P, C_A^P and x_P, and these are fixed by a thermodynamic relation between C_O^P and C_A^P (e.g., a solubility product for dilute solutions) and two mass conservation conditions. In the above manner, an actual diffusion path is obtained as shown in Fig. 4.

It is worthwhile clarifying the role that ternary diffusional interaction plays in producing internal oxidation. For illustrative purposes, it is assumed that the solubility curve for oxygen in alloy AB involves a minimum as shown in Fig. 5. Consider the "virtual" diffusion paths designated (1) and (2). In case (1) a maximum in the oxygen distribution in the alloy has resulted in a maximum in the "virtual" diffusion path for the alloy. As a consequence of this, it is possible for the virtual path to cut into the two-phase field, thus producing supersaturation and a driving force for phenomena such as internal oxidation and morphological breakdown. A maximum in the oxygen distribution (or diffusion path) requires that there be strong diffusional

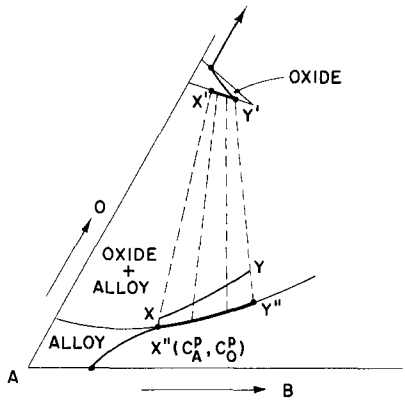

Fig. 4. A situation which involves a zone of internal oxidation in the alloy. The variations in the composition of the internal oxide and the alloy matrix are given by X'Y' and X''Y'' respectively. The line XY represents the average composition of the subscale region.

interaction with the other independent species in the alloy. In the section on ternary diffusion equations, it was noted that the tendency for such interaction is enhanced by strong chemical interaction between A and O, a very steep distribution of A and a very shallow distribution of O. Note that in case (2), unlike case (1), it is not necessary to have diffusional interaction in order to produce supersaturation.

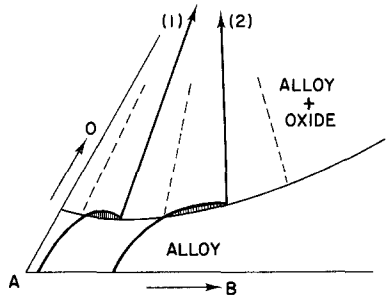

Fig. 5. Two "virtual" diffusion path possibilities which illustrate the influence of ternary diffusion interaction. Cases (1) and (2) involve regions of the oxygen solubility curve which have negative and positive slopes, respectively.

ALLOY–OXIDE INTERFACE STABILITY

In the previous section, it was indicated that if the "virtual" diffusion path for the alloy cuts through the two-phase field (alloy + oxide) as in Fig. 3(b), then a thermodynamic driving force exists for internal oxidation within the alloy and for morphological breakdown of a planar alloy–oxide interface. The most rigorous approach to morphological stability problems involves the application of mathematical perturbation methods. One introduces a small shape perturbation into an initially planar interface and then solves the pertinent differential equations to decide the fate of this perturbation. If it grows with time, the interface is unstable. On the other hand, if the perturbation decays with time, the interface will maintain a stable planar shape. Wagner[15,30] has employed these methods on a certain limiting (pseudobinary) situation, while Coates and Kirkaldy[31] have more recently generalized the treatment for application to systems of arbitrary constitution. The latter study revealed that there are situations in which it is possible to maintain a planar alloy–oxide interface, in spite of supersaturation in the alloy. In contrast, it also was found that there are situations in which an alloy–oxide interface will break down in the absence of any supersaturation. That is to say, an alloy–oxide interface can be unstable for purely kinetic reasons, the limit treated by Wagner. In the present article, the authors do not wish to initiate a detailed discussion of this complex problem. However, on the basis of rather simple arguments, it can be demonstrated[30] that if the oxidation rate is determined exclusively by mass transport in the oxide, the scale–alloy interface will maintain a stable planar shape. On the other hand, if the rate-determining process is transport in the alloy, there is a very strong tendency for a planar scale–alloy interface to break down to a nonplanar morphology.

These qualitative stability criteria arise out of the assumption that transport in one or other of the phases is rate determining. This assumption is reasonable only for extreme limiting cases. For more general cases rather sophisticated techniques, such as the perturbation methods, are required.

If a planar scale–alloy interface is morphologically stable, any supersaturation developed in the alloy can be relieved by internal oxidation only. On the other hand, if the interface is not stable in the presence of supersaturation, both morphological breakdown and internal oxidation are possible.

APPLICATIONS

In this section we consider specific systems and use the principle of superposition of the "virtual" or the actual diffusion path onto the appropriate ternary phase diagram. Smeltzer and Perrow[32,33] have used this

method in the analysis of oxidation of Fe–Ni and Fe–Cr alloys. We hope to illustrate how this technique provides a means of appraising the role played by both kinetic (diffusion) and thermodynamic parameters involved in the oxidation of binary alloys.

We consider first the oxidation of binary iron alloys, Fe–B, and inquire into the role played by the alloying element B. Alloying elements in iron may decrease the rate of oxidation by lowering the composition range of wustite or by eliminating it as a stable phase in the presence of the alloy and spinel phases. Additional protection may be obtained if the alloying element lowers the range of defect concentration in the spinel phase or decreases the ion mobilities. Alternatively, protection may be obtained if B is sufficiently reactive that its oxide is the only constituent of the external scale and is adherent and resistant to diffusion of ionic species, as in the case of Cr_2O_3 formed on Fe–Cr alloys.[34]

The effect of the alloying element B is best understood by considering the ternary phase diagram Fe–B–O. Substantial information on ternary Fe–Ni–O and Fe–Cr–O phase diagrams at 1000°C is now available (Figs. 6 and 7). One may note certain common features in these diagrams. The alloy side of the diagram is divided into three regions by points A_1 and A_2. Wustite is the oxide that coexists with alloy up to the point A_1. Between points A_1 and A_2, a spinel phase becomes the stable oxide phase and beyond

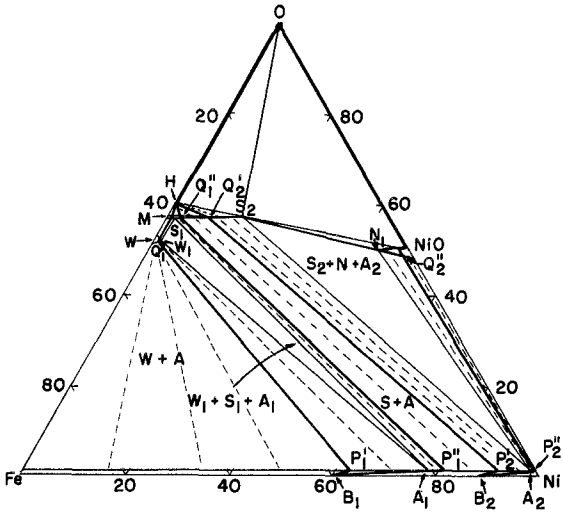

Fig. 6. 1000°C isotherm of the Fe–Ni–O system in atomic percent[35–37] and possible diffusion paths for alloy compositions B_1 and B_2. W_1—$Fe_{0.87}Ni_{0.01}O$; S_1—$Ni_{0.04}Fe_{2.96}O_4$; S_2—$NiFe_2O_4$; N_1—$Ni_{0.87}Fe_{0.13}O$; A_1—79.6 at.% Ni, 20.4 at.% Fe; A_2—99.5 at.% Ni, 0.5 at.% Fe.

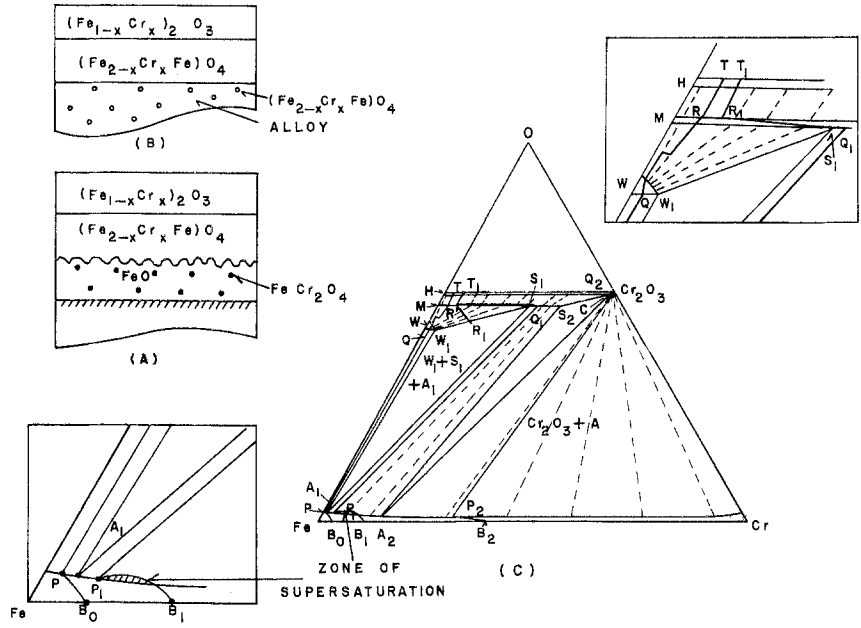

Fig. 7. Schematic representation of the scale structures corresponding to the oxidation of (a) a *very* dilute Fe–Cr alloy (after Moreau[38]) and (b) a dilute Fe–Cr alloy.[39] (c) 1000°C isotherm of Fe–Cr–O system (at.%)[40,41] and possible diffusion paths corresponding to the oxidation of Fe–Cr alloys. W_1—$Fe_{0.97}Cr_{0.02}O$; S_1—$Fe_{1.5}Cr_{1.5}O_4$; S_2—$FeCr_2O_4$; C—<1 at.% Fe; A_1—<1 at.% Cr; A_2—13.6 at.% Cr, 76.4 at.% Fe. Insert at the top right shows the oxide region on an expanded scale.

point A_2, the oxide of the alloying element becomes the staple phase co-existing with the alloy. Points A_1 and A_2 are vertices of the wustite–spinel–alloy and spinel–BO–alloy three-phase fields respectively. The stability ranges with respect to alloy composition, of wustite and the oxide BO of the alloying element, will depend on their relative free energies of formation. In the Fe–Ni–O system (Fig. 6) wustite has a much larger negative free energy of formation than nickel oxide and therefore the stability range of the former extends up to 80 at.% Ni in the alloy whereas the stability range of the latter is almost negligible (0–0.5 at.% Fe). Replacement of Ni by a more reactive component such as Cr reduces the stability range of wustite with respect to the alloy composition to a negligible value and extends the stability range of BO, i.e., Cr_2O_3 (Fig. 7). Thus as increasingly more reactive elements are introduced as component B in Fe–B, points A_1 and A_2 shift toward the iron corner of the phase diagram. This demonstrates the significant effect of the alloying element B on oxide stability.

Internal Oxidation and Morphological Breakdown

In the literature, the terms internal oxide and subscale have been used with different meanings and at other times interchangeably. In the present paper, the term internal oxide is used to describe discrete precipitation of oxide of the solute or the solvent metal or a mixed oxide of these within the alloy matrix. The term subscale is used in a more general sense to describe the internal oxide as well as any zone below the external scale which contains both the alloy and oxide phases (usually resulting from instability of the system).

In discussing the phenomenon of internal oxidation, Wagner[17,24] has considered only limiting cases in which the free energies of oxidation of metals A and B are sufficiently different that one of them, say A, acts as a noble metal and the other, B, is very reactive. In his review of the phenomenon of internal oxidation, Rapp[29] considered two cases for dilute alloys of B in A: (1) internal oxidation without external scale, and (2) internal oxidation with external scale. Each of these two cases can be easily understood in terms of the "virtual" diffusion path concept.

We first consider case (1), internal oxidation without external scale, a good example being in the Ag–In system.[29] In Fig. 8(a), B_0 represents the bulk alloy composition which corresponds to dilute solution of metal B in metal A. For the sake of clarity, the oxygen solubility line PRS, etc., is exaggerated. If metal A does not form an oxide at the temperature of oxidation and the activity of metal B in the alloy phase is small enough that the oxide BO also does not form as an external scale, then the "virtual" diffusion path corresponds to $OPQSB_0$ in Fig. 8(a). Line PQ is almost horizontal because oxygen diffusion through the alloy is much faster than for B. The zone of supersaturation PQS will lead to internal precipitation of BO. After internal precipitation, the diffusion path within the alloy matrix

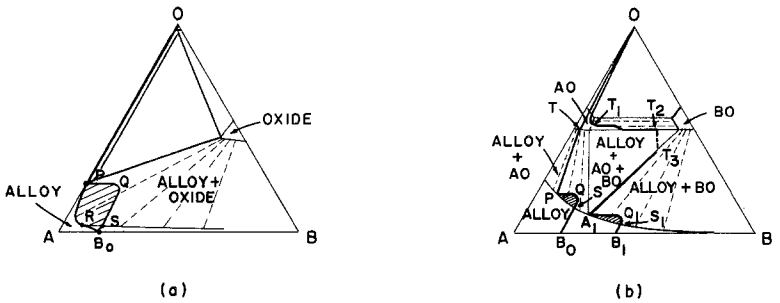

Fig. 8. (a) Diffusion path corresponding to the case of internal oxidation without an external scale. (b) Possible diffusion paths corresponding to the case of internal oxidation with external scale.

shifts to PRB_0; part PR corresponds to the internal oxidation zone in which the concentrations of B and O are reduced to relatively small values and part RB_0 corresponds to the steep rise in concentration of B to the bulk concentration value B_0 beyond the internal oxidation zone. The phase diagram tie lines yield the local compositions of the alloy matrix and precipitate phase BO.

Let us now consider case (b) in which internal oxidation occurs in conjunction with an external scale. This situation is schematically represented in Fig. 8(b). $OTPQSB_0$ is the diffusion path for the simplest case wherein both the external scale and internal oxide precipitate are AO. The Cu–Pd system exhibits this type of internal oxidation behavior.[2,24] A more complex but frequently observed case is that in which the external scale consists of a single-phase zone of oxide AO and then a two-phase AO-BO zone followed by an internal oxidation zone consisting of BO precipitate particles in the alloy matrix. This case corresponds to the diffusion path $OT_1T_2T_3A_1Q_1S_1B_1$ in Fig. 8(b). Note that in this case, the diffusion path passes through the three-phase field AO + A_1 + BO (the segment T_2T_3) and this represents the interface between the two-phase AO-BO region and the internally oxidized alloy. An example of this case occurs for dilute Cu–Be alloys.[29] These alloys show a tendency to form a single external layer of oxide BO at higher concentrations of metal B in the bulk alloy.

Oxidation of Fe–Ni Alloys*

For dilute Fe–Ni alloys (0–20% Ni), despite the presence of wustite in the external scale, the oxidation rates drop drastically with respect to the rate for pure iron. Because the solubility of nickel in wustite is almost negligible, nickel enrichment occurs in the alloy adjacent to the oxide–alloy interface. This enrichment can be extremely high. Menzies and Tomlinson[42] observed up to 15% Ni at the wustite–alloy interface for Fe–2.3% Ni alloys and 65% Ni at the interface for Fe–48% Ni alloys, after only 30 min of oxidation. Brabers and Birchenall,[43] Morris and Smeltzer,[44] and Wulf *et al.*[45] also observed similar enrichment. This enrichment of nickel at the interface results in the diffusion path in the alloy shifting toward the nickel side of the phase diagram[32,43] (e.g., $B_1P'_1$, and $B_1P''_1$, in Fig. 6).

One can see that the composition range of wustite is reduced as the Ni content is increased. As a result, the driving force for diffusion through wustite is reduced and therefore the oxidation rate is lowered. Formation of wustite is dependent upon a supply of iron at the wustite–alloy interface. Because there is a depletion of iron in the alloy at this interface, then due to

*The alloy compositions cited in the following sections are understood to be in weight percent unless otherwise stated.

relatively slow diffusion of Fe and Ni in the alloy, the oxidation rate is further reduced from that of pure Fe.

Let us consider in more detail the possible configurations which are expected during oxidation of Fe–Ni alloys. Neglecting subscale formation for the moment, one obtains the diffusion path $B_1P'_1Q'_1$ etc. for a situation in which wustite is present in the external scale. Notice that due to Ni enrichment the path swings toward the Ni corner of the diagram. It is possible that Ni enrichment in the alloy near the interface could push the interface alloy composition beyond A_1 and wustite would no longer be stable. The diffusion path corresponding to this situation is $B_1P''_1Q''_1$ etc., which involves spinel in the external scale. For an alloy with bulk composition B_2 we may observe either the diffusion path $B_2P'_2Q'_2$ etc., corresponding to formation of spinel in the external scale or alternatively the diffusion path $B_2P''_2Q''_2$ etc., where the interfacial alloy composition has shifted beyond A_2 so that nickel oxide becomes the stable oxide.

The above semiquantitative description of Fe–Ni alloy oxidation compares very favorably with experiments. Wulf *et al.*[45] have found that for Fe–Ni alloys containing up to 20% Ni, wustite is present in the external scale. This corresponds to the diffusion path $B_1P'_1Q'_1$ etc. For alloys containing 20–35% Ni it was observed that spinel is the oxide present in the external scale. This corresponds to the diffusion path $B_1P''_1Q''_1$ etc. See also Ref. 32.

Subscale Formation During the Oxidation of Fe–Ni Alloys

We have seen that for Fe–Ni alloys with bulk composition B_1 such that $0 < \text{Ni}(B_1) < \text{Ni}(A_1)$, two types of diffusion paths exist, one corresponding to the presence of wustite in the external scale and the other to the presence of spinel in the external scale. One would expect different subscale formations in these cases. Consider first subscale formation when wustite appears in the external scale. The diffusion path corresponding to this situation is shown in Fig. 9(c), $B_1R_1Q_1$, etc. As we have noted earlier, formation of wustite leads to a depletion of iron in the alloy at the interface. This results in a steep iron concentration gradient as shown in Fig. 9(a). This gradient, combined with an oxygen solubility which increases with Ni content and a fast rate of oxygen diffusion in the alloy, gives rise to a zone of supersaturation in the alloy. The supersaturation provides a driving force for internal oxidation and/or morphological instability. Notice that the iron concentration in wustite is much higher than that in the alloy at the wustite–alloy interface. In addition, the diffusion of iron through wustite is several orders of magnitude higher than its diffusion through the alloy.[47] Therefore the wustite–alloy interface should be morphologically very unstable according to the

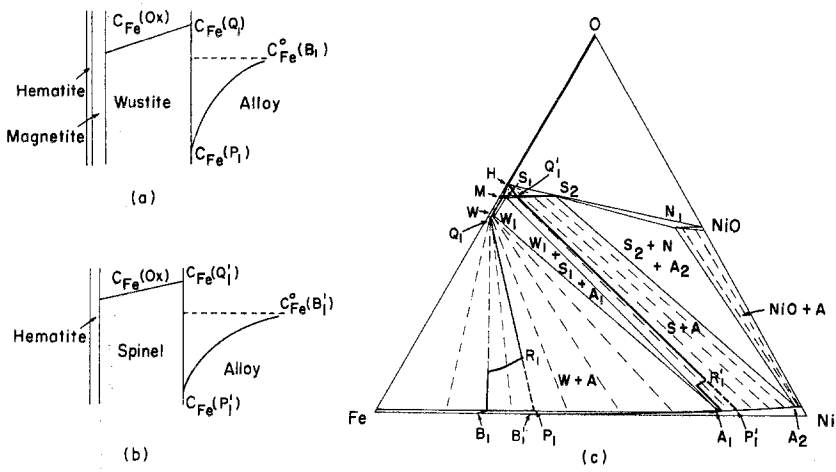

Fig. 9. (a) and (b) are respectively, schematic representations of scale structures and Fe concentration profiles for bulk alloy compositions B_1 and B'_1. (c) corresponding actual diffusion paths.

criteria we have discussed earlier in the section on morphological stability. In summary, subscale formation is expected to occur by both internal precipitation and morphological instability of the oxide–alloy interface. That such is the case is suggested by the micrographs in Refs. 44 and 45. It is apparent from earlier discussions that the diffusion path within the alloy matrix would go along the oxygen solubility line after the internal precipitation has occurred. Point P_1 in Fig. 9(c) corresponds to the composition of alloy with maximum depletion of iron; this alloy is in equilibrium with the external scale.

Oxidation of Fe–Ni alloys containing 20–35% Ni is very interesting.[45] The diffusion path for these alloys, $B'_1R'_1Q'_1$ etc., is shown in Fig. 9(c). From the diffusion path it is clear that the external scale for such alloys would consist of hematite and spinel. The interfacial alloy composition has shifted to P'_1, beyond A_1. The zone of supersaturation is in the two-phase field spinel + alloy and thus the internal oxide is expected to be spinel. According to Wulf *et al.*, wustite does not appear as the internal oxide for these alloys. The concentration profile for Fe, corresponding to the diffusion path in Fig. 9(c) is shown in Fig. 9(b). This distribution appears to be almost identical to the case in which wustite is present in the external scale and hence one might again expect to observe morphological instability. However, after noting the fact that diffusion of iron through nickel-rich spinel is slower than that in the alloy,[46] we see that the criteria for occurrence of morphological instability (as discussed earlier) are not satisfied. Hence,

one expects to observe only internal oxidation, as is indicated by the observations of Wulf *et al.* It should be noted that for alloys containing lower Ni, the spinel formed in the external scale contains very little Ni, resulting in higher cationic mobilities. This may lead to morphological instability of the oxide–alloy interface for these alloys.

Oxidation of Fe–Cr Alloys

In connection with the oxidation of Fe–Ni alloys we have seen that due to selective oxidation, the diffusion path in the alloy is biased toward the Ni corner. This bias is thus toward the more noble element. In the oxidation of Fe–Cr alloys, since Cr preferentially oxidizes, the diffusion path should shift toward Fe. Thus, although it appears from the Fe–Cr–O phase diagram (Fig. 7) that wustite is not stable for almost the complete bulk alloy composition range, it may in fact become a stable phase due to the interface alloy composition shift toward the Fe corner of the phase diagram.

Because the oxidation of dilute Fe–Cr alloys is of such commercial importance, let us examine the problem more carefully. Figure 7(a) shows the oxide scale structure for a very dilute alloy as observed by Moreau.[38] In Fig. 7(c) is shown a possible diffusion path for a very dilute Fe–Cr alloy ($B_0 < 1\%$ Cr) which has wustite in the scale. The segment of this diffusion path OT corresponds to the equilibrium at the scale–gas interface. The diffusion path then passes through the single phase Fe_2O_3–Cr_2O_3 solid solution region, which corresponds to the presence of this phase, $(Fe_{1-x}Cr_x)_2O_3$, in the oxide scale. The segment TR represents the equilibrium between the solid solution $(Fe_{1-x}Cr_x)_2O_3$ and the spinel phase $(Fe_{2-x}Cr_xFe)O_4$. The passage of the diffusion path through the spinel phase field corresponds to the presence of this phase in the scale. If the actual diffusion path were subsequently to follow a tie line in the two-phase field wustite–spinel, then we would obtain a planar interface between spinel and wustite and a wustite layer with no precipitate particles in it. However, a two-phase "$FeCr_2O_4$"–FeO region is indicated in Fig. 7(a) and therefore the actual diffusion path must cut across tie lines in the two-phase wustite–spinel field. This explains the two-phase region of spinel precipitate particles in wustite. From the phase diagram, it can be seen that the spinels in equilibrium with wustite vary in composition from Fe_3O_4 to $Fe_{1.5}Cr_{1.5}O_4$. It follows that any spinel precipitate which coexists with wustite must have a composition in this range if the assumption of local equilibrium is valid.

As the bulk alloy composition is moved further away from the Fe corner of the phase diagram, it is expected that wustite is eventually eliminated

as a stable phase. Only a trace of chromium is required at the alloy–oxide interface to stabilize the spinel phase. Experimental evidence on the scale structure of oxidized dilute iron–chromium alloys (e.g., Fe–5% Cr) is conflicting. Some investigators[38,47] have found wustite occurring in the external scale, while others[33,39] report no such occurrence. Careful consideration of the experimental results indicates that the wustite phase may be stabilized due to impurities such as Mn. The diffusion path corresponding to the situations in which there is an inner spinel layer and an outer ferric–chromic oxide layer [Fig. 7(b)] is shown in Fig. 7(c), $B_1P_1Q_1R_1T_1O$.

It is interesting to note the interplay between the thermodynamic and kinetic factors which results in this unique diffusion path. Due to the high reactivity of Cr, it tends to preferentially oxidize, resulting in Cr depletion in the alloy adjacent to the oxide–alloy interface. However, since the diffusion coefficient of Cr in γFe–Cr alloys is small, Cr cannot reach the interface very rapidly. On the other hand, for thermodynamic equilibrium at the oxide–alloy interface, the Cr content in the spinel phase has to be relatively high. The thermodynamic and kinetic factors thus militate against each other, resulting in a steep Cr gradient in the spinel, shifting the diffusion path sharply toward the Fe corner. The Cr content of the ferric–chromic oxide in equilibrium with the spinel phase is thus very low. The low Cr content of the ferric–chromic oxide balances the high Cr content of spinel, resulting in relatively small net excess of Cr in the entire duplex oxide scale and hence a small depletion of Cr in the alloy. Note that because the diffusivity of Cr in the alloy is low and the rate of thickening of the scale is relatively high, the existence of a scale containing a ferric–chromic oxide of high Cr content violates the principle of mass conservation.

For Fe–Cr alloys containing concentrations greater than about 13 at.% Cr, the diffusion path is uncomplicated, viz., $B_2P_2Q_2O$. Thus Cr_2O_3 is the only oxide formed in the external scale. Formation of Cr_2O_3 depletes the alloy of Cr and therefore shifts the diffusion path toward the Fe corner of the phase diagram. However, since Cr_2O_3 is highly adherent to the alloy and resistant to diffusion, further oxidation is very slow. Clearly the diffusion path shift toward the Fe corner, B_2P_2, must not be beyond the point A_2.

Oxidation of Ni–Cr Alloys

The Ni–Cr–O phase diagram [Fig. 10(b)] is similar to the Fe–Cr–O diagram. Since nickel is more noble than iron, the points A_1 and A_2 are situated nearer the Ni corner as compared to their equivalent position on the Fe–Cr–O diagram. Thermodynamic calculations[29,48] suggest that point A_1 corresponds to only a trace of Cr in the alloy and point A_2 corresponds to less than 1 at.% Cr. Therefore most of the alloy composition range lies

adjacent to the two-phase field alloy + Cr_2O_3. Croll and Wallwork[49] have recently suggested that point A_2 corresponds to 10 at.% Cr. This observation appears to be in disagreement with the thermodynamic calculations[29,48] and with the numerous observations of a Cr_2O_3 internal oxide coexisting with virtually pure Ni matrix during the oxidation of dilute Ni–Cr alloys at 1000°C.[48,50–52] However, if one accepts the suggestion of Croll and Wallwork, the identity of the internal oxide particles or the validity of the local equilibrium assumption is in question. Further experimental work is required in order to resolve the discrepancy. For the purpose of the present work, the theoretical values for the compositions corresponding to the points A_1 and A_2 are assumed since these are more in accord with the experimental observations and the thermodynamic data on the Ni–Cr alloy system.

Oxidation of dilute Ni–Cr alloys has been studied by Moreau and Benard,[50] Birks and Richert,[48] Pfeiffer,[53] and Douglass.[54] Additions of Cr to Ni increase the oxidation rate until about 8% Cr. The oxidation rate then decreases abruptly and is about equal to that of pure Ni at 10% Cr. Chromium additions of about 20% markedly reduce the oxidation rate by the formation of Cr_2O_3 in lieu of a film of NiO.[54]

Moreau and Benard[50] have studied the oxidation of an Ni–5% Cr alloy. The oxide scale structure for such an alloy at 1000°C is shown in Fig. 10(a). Because the point A_2 corresponds to less than 1 at.% Cr, the

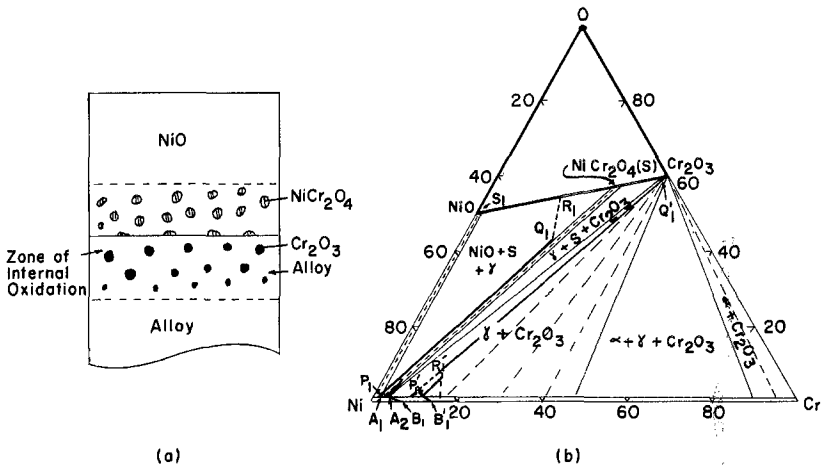

Fig. 10. (a) Schematic representation of scale structure corresponding to oxidation of an Ni–5% Cr alloy at 1000°C. (b) Possible diffusion paths corresponding to the oxidation of Ni–Cr alloys at 1000°C plotted on the 1000°C isotherm of the Ni–Cr–O system (at.%); A_1—$\ll 1$ at.%; A_2—< 1 at.%; Solubilities of NiO and Cr_2O_3 in each other are small. The extent of the spinel phase is very small (near $NiCr_2O_4$) and is exaggerated for the purpose of illustration.

existence of complex scale structures [such as shown in Fig. 10(a)] for Ni–Cr alloys containing less than 8% Cr must be due to the shift of the diffusion path in the alloy toward the Ni corner of the isotherm. A possible diffusion path for such an alloy (bulk composition B_1) is $B_1Q_1R_1S_1O$, Fig. 10(b). The system is apparently unstable with respect to NiO–$NiCr_2O_4$, i.e., these phases cannot coexist at a planar interface. The breakdown of the interface eventually leads to formation of a two-phase zone NiO–$NiCr_2O_4$. The interface between the zone of internal oxidation and NiO–$NiCr_2O_4$ region corresponds to the dotted line R_1Q_1 in Fig. 10(b).

It appears from the experimental results that for Ni–Cr alloys containing more than 15% Cr, the Cr depletion in the alloy is not sufficient to shift the interfacial alloy composition beyond point A_2. For these alloys, the diffusion path is $B_1'R_1'Q_1'O$ in Fig. 10(b), corresponding to formation of a single Cr_2O_3 layer and a Cr_2O_3 internal precipitate in the alloy. The adherence of Cr_2O_3 to the alloy, its compactness and diffusion resistance, result in this oxide being very protective. The diffusion path $B_1'R_1'Q_1'O$ is an experimental diffusion path corresponding to concentration profiles given by Wood and Hodgkiess.[55]

CONCLUSIONS

An attempt has been made in this work to rationalize the complex processes that occur during the oxidation of binary alloys. The assumption of local equilibrium is essential to the whole argument. Considering the fact that each change must bring the system, both generally and locally, closer to equilibrium, this seems to be the most realistic assumption to start with. It is also assumed in this analysis that the oxide layers are free of pores and cracks, have uniform thickness, and are adherent to the alloy substrate. Although this is a highly idealized model, one recognizes the need to rationalize to the maximum extent the oxidation of binary alloys in terms of the ternary alloy–oxygen equilibria and the transport processes within the alloy and the mixed oxide systems.

In the present analysis two-phase regions are treated as being formed due to the morphological instability of the planar interface between two single-phase regions or due to the occurrence of supersaturated regions within a single-phase field. Although the method seems to be the most appropriate for the analysis within the alloy matrix, it may not be the only way to consider two-phase fields in the oxide scale. Wagner[16] has considered simultaneous nucleation and growth of two phases to form a two-phase region. This treatment could be extended to a generalized ternary analysis.

During any attempt at a mathematical analysis of the problem of oxidation of alloys, a lack of knowledge of the thermodynamic and the transport properties of the mixed oxide systems is felt. In a mixed oxide system, there may be interactions among like and unlike defects such as the vacancies and the solute atoms. These interactions profoundly influence the thermodynamic and the transport properties of these systems. The Wagner-Hauffe rules do not provide a useful guideline in considering transport through such systems as FeO–NiO or NiO–CoO. The Wagner-Schottky model of nonstoichiometric crystals becomes too approximate for such grossly defective oxides as FeO or CoO, or for concentrated oxide solutions.[56–58] However, no general statistical theory of mixed oxide systems is as yet available. The specific information that is needed in the analysis of the oxidation of alloys concerns the effect of the cation and anion activities on the defect structures of a mixed oxide system, the variation of cation activities with composition and also the functional form of the concentration dependence of the diffusion coefficients of the mobile species in the oxides. Apart from this, data on the shape of the oxygen solubility curves for various alloy systems are highly desirable for an analysis of the phenomena of internal oxidation and morphological breakdown.

At present, a general theoretical treatment to consider the oxidation of binary alloys is available.[18–20] The electron microprobe provides us with a powerful method to investigate the oxide scale structures, the cation distribution in the oxide, and the distribution of the metallic components in the alloy. Together they should help considerably in investigations in the near future.

ACKNOWLEDGMENTS

The authors are grateful to Professor W. W. Smeltzer for a critical review of the original manuscript. Professors W. W. Smeltzer and J. S. Kirkaldy and their co-workers contributed greatly via stimulating discussions. The authors wish to acknowledge scholarship support from the International Nickel Company of Canada Ltd. (A.D.D.) and the Steel Company of Canada Ltd. (D.E.C.).

REFERENCES

1. F. N. Rhines, *Trans. AIME* **137**, 246 (1940).
2. D. E. Thomas, *Trans. AIME* **191**, 926 (1951).
3. J. B. Clark and F. N. Rhines, *Trans. ASM* **51**, 199 (1959).
4. J. S. Kirkaldy and L. C. Brown, *Can. Met. Quart.* **2**, 89 (1963).
5. J. S. Kirkaldy, *Adv. Mat. Research* **4**, 55 (1970).
6. J. S. Kirkaldy in *Oxidation of Metals and Alloys* (ASM Monograph, Cleveland, 1971), pp. 101–114.

7. L. Onsager, *Ann. N.Y. Acad. Sci.* **46**, 241 (1945).
8. G. J. Hooyman, S. R. De Groot, and P. Masur, *Physica* **21**, 360 (1955).
9. J. G. Kirkwood, R. L. Baldwin, P. J. Dunlop, L. J. Gosting, and G. Kegeles, *J. Chem. Phys.* **33**, 1505 (1960).
10. D. G. Miller, *Chem. Rev.* **60**, 15 (1960).
11. J. E. Lane and J. S. Kirkaldy, *Can. J. Phys.* **42**, 1643 (1964).
12. J. S. Kirkaldy and G. R. Purdy, *Can. J. Phys.* **40**, 208 (1962).
13. F. N. Rhines, W. A. Johnson, and W. A. Anderson, *Trans. AIME* **147**, 205 (1942).
14. C. Wagner, *J. Electrochem. Soc.* **99**, 369 (1952).
15. C. Wagner, *J. Electrochem. Soc.* **103**, 571 (1956).
16. C. Wagner, *J. Electrochem. Soc.* **103**, 627 (1956).
17. C. Wagner, *Z. Elektrochem.* **63**, 772 (1959).
18. C. Wagner, *Corr. Sci.* **9**, 91 (1969).
19. D. E. Coates and A. D. Dalvi, *Oxidation of Metals* **2**, 331 (1970).
20. A. D. Dalvi and D. E. Coates, *Oxidation of Metals* **3**, 203 (1971).
21. J. W. Rutter and B. Chalmers, *Can. J. Phys.* **31**, 15 (1953).
22. W. A. Tiller, K. A. Jackson, J. W. Rutter, and B. Chalmers, *Acta Met.* **1**, 428 (1953).
23. L. S. Darken, *Trans. AIME* **150**, 157 (1942).
24. C. Wagner, *Corrosion Sci.* **8**, 887 (1968).
25. M. Kahlweit, *Z. Phys. Chem. N.F.* **32**, 1 (1962).
26. G. Böhm and M. Kahlweit, *Acta Met.* **12**, 641 (1964).
27. P. Bolsaitis and M. Kahlweit, *Acta Met.* **15**, 765 (1967).
28. J. S. Kirkaldy, *Can. Met. Quart.* **8**, 35 (1969).
29. R. A. Rapp, *Corrosion* **21**, 382 (1965).
30. C. Wagner, *Z. Elektrochem.* **63**, 958 (1959).
31. D. E. Coates and J. S. Kirkaldy, *Trans. ASM* **62**, 426 (1969).
32. W. W. Smeltzer, *Trans. Can. Min. Met. Soc.* **65**, 367 (1962).
33. J. M. Perrow and W. W. Smeltzer, *J. Electrochem. Soc.* **109**, 1023 (1962).
34. C. E. Birchenall, *Z. Elektrochem.* **63**, 790 (1959).
35. A. D. Dalvi and W. W. Smeltzer, *J. Electrochem. Soc.* **117**, 1431 (1970).
36. G. S. Viktorovich and D. I. Lisovskii, *Tsvetnye Metally* **7**, 49 (1966).
37. G. S. Viktorovich, V. A. Gutin, and D. I. Lisovskii, *Tsvetnye Metally* **7**, 54 (1966).
38. J. Moreau, *Publ. Inst. Recherches Siderurgie* (A), No. 49 (1953).
39. D. Lai, R. J. Borg, M. J. Brabers, J. D. Mackenzie, and C. E. Birchenall, *Corrosion* **17**, 357 (1961).
40. A. U. Seybolt, *J. Electrochem. Soc.* **107**, 147 (1960).
41. C. T. Fujii and R. A. Meussener, *Trans. AIME* **242**, 1259 (1969).
42. L. A. Menzies and W. J. Tomlinson, *JISI* **204**, 1239 (1958).
43. M. J. Brabers and C. E. Birchenall, *Corrosion* **14**, 179t (1958).
44. L. A. Morris and W. W. Smeltzer, *Acta Met.* **15**, 1591 (1967).
45. G. L. Wulf, T. J. Carter, and G. R. Wallwork, *Corrosion Sci.* **9**, 689 (1969).
46. Karl Hauffe, *Oxidation of Metals* (Plenum Press, New York, 1965), p. 45.
47. H. J. Yearian, E. G. Randell, and T. A. Longo, *Corrosion* **12**, 515t (1956).
48. N. Birks and H. Rickert, *J. Inst. Met.* **91**, 308 (1962).
49. J. E. Croll and G. R. Wallwork, *Oxidation of Metals* **1**, 55 (1969).
50. J. Moreau and J. Benard, *Compt. Rend.* **237**, 1417 (1953).
51. C. G. Giggins and F. S. Pettit, *Trans. AIME* **245**, 2495 (1969).
52. G. C. Wood, *Oxid. Metals* **2**, 11 (1970).
53. Von Irmtraud Pfeiffer, *Z. Metallkde.* **51**, 322 (1960).
54. D. L. Douglass, *Corrosion Sci.* **8**, 665 (1968).
55. G. C. Wood and T. Hodgkiess, *J. Electrochem. Soc.* **113**, 319 (1966).
56. N. N. Greenwood, *Ionic Crystals, Lattice Defects and Nonstoichiometry* (Butterworths, London, 1968), Ch. 6.
57. J. S. Anderson, *Proc. Chem. Soc.*, 166 (1964).
58. R. F. Goulet, ed., *Nonstoichiometric Compounds*, Adv. Chem., Series 39 (American Chemical Society, Washington D.C., 1963).